

Effect of flow shear on the onset of dynamos

Shishir Biswas^{1,2,*} and Rajaraman Ganesh^{1,2,†}

¹*Institute for Plasma Research, Bhat, Gandhinagar, Gujarat 382428, India*

²*Homi Bhabha National Institute, Training School Complex, Anushaktinagar, Mumbai 400094, India*

(Dated: June 1, 2023)

Understanding the origin and structure of mean magnetic fields in astrophysical conditions is a major challenge. Shear flows often coexist in such astrophysical conditions and the role of flow shear on dynamo mechanism is only beginning to be investigated. Here, we present a direct numerical simulation (DNS) study of the effect of flow shear on dynamo instability for a variety of base flows with controllable mirror symmetry (i.e, fluid helicity). Our observations suggest that for helical base flow, the effect of shear is to suppress the small scale dynamo (SSD) action, i.e, shear helps the large scale magnetic field to manifest itself by suppressing SSD action. For non-helical base flows, flow shear has the opposite effect of amplifying the small-scale dynamo action. The magnetic energy growth rate (γ) for non-helical base flows are found to follow an algebraic nature of the form, $\gamma = -aS + bS^{\frac{2}{3}}$, where $a, b > 0$ are real constants and S is the shear flow strength and γ is found to be independent of scale of flow shear. Studies with different shear profiles and shear scale lengths for non-helical base flows have been performed to test the universality of our finding.

I. INTRODUCTION

Predicting the generation of multi-scale magnetic fields, in many astrophysical bodies, has been a long-standing theoretical question in astrophysical plasmas. Different theories have been proposed to account for the origin of these multi-scale magnetic fields. For example, invoking magnetic induction due to the motion of conducting fluids,^{1,2} suggested these multi-scale magnetic fields are generated via a hydromagnetic dynamo process and maintained against resistive losses.

Depending on the length scales involved, dynamos may be classified into two broad categories : Small Scale or fluctuation Dynamo (SSD) and Large Scale or mean field Dynamo (LSD). Unlike SSD, for LSDs a lack of reflectional symmetry is widely believed to be a necessary condition³. Depending on the time scales, dynamos may also be categorized as Fast dynamos (growth rate remain finite in the range $R_m \rightarrow \infty$) and Slow dynamos (magnetic diffusion plays a significant role)^{3,4}. Fast dynamos are further classified into two sub-categories as, ‘quick’ dynamo and ‘pedestrian’ dynamo⁵. For a ‘quick’ dynamo magnetic energy growth rate achieves its maximum value quickly as a function of magnetic Reynolds number R_m , where as for a ‘pedestrian’ dynamo the growth rate very weakly depends on R_m ⁵. Depending on the feedback strength of the magnetic field on to the flow field, dynamos are regarded as linear or non-linear. For example, a linear dynamo is one in which the magnetic field dynamics does not “back react” with the velocity field and the velocity field is either given or it obeys the Navier-Stokes equation³. A nonlinear dynamo or self-consistent dynamo is when the nonlinear effects start to change the flow (once the magnetic field is large enough) to stop fur-

ther magnetic field growth, that is, the flow and B-field “back react” on each other, typically leading to nonlinear saturation³.

SSDs may also be defined as systems which sustain B-field fluctuations at scales smaller than the forcing scale⁶⁻¹¹. The fluctuating magnetic fields found in galaxies and clusters, as well as in the solar photosphere may be regarded as due to SSDs. Oftentimes, the generated magnetic fields are also observed to be correlated on scales larger than the driving scale, resulting in LSD action^{3,12}. For instance, the solar magnetic field possesses a large-scale dipole component which is mostly aligned with the Sun’s rotation axis and a wave of magnetic activity that traverses from mid-latitudes to the equator on an 11-year time scale is clearly visible in the solar butterfly diagram¹³. Large-scale dynamo activity can also be explained by the well-known α effect^{2,3,14}, provided the system has some mirror-symmetry breaking (i.e, when kinetic or fluid helicity is non-zero).

Not only by the nature of turbulence, but, dynamos are also affected by factors such as density lamination (for example, density variation along the direction of gravity), rotation, kinetic helicity (mirror symmetry breaking), and flow shear. Out of these factors, flow shear is ubiquitous in astrophysical systems - appearing in interstellar medium, galaxies, accretion disks, and in liquid-metal laboratory dynamo¹⁵ experiments. The paradigm of investigation of the exponential growth of magnetic field caused by the interaction of small-scale velocity fluctuations and a large-scale velocity shear; is commonly referred to as the “shear dynamo problem”. For example, presence of a large-scale velocity shear, in association with turbulent rotating convection (turbulent convective motion under the influence of rotation), is seen to actually increase the dynamo growth rate at larger scales¹⁶⁻¹⁹. Furthermore, it is also found that a highly helical flow pattern may only result in a SSD action when the rotational convention is sufficiently strong²⁰.

For conditions where rotational effects are negligible,

* shishirbeafriend@gmail.com; shishir.biswas@ipr.res.in

† ganesh@ipr.res.in

an integro-differential equation has been proposed based on a quasi-linear model to address the limit of weak convective flow^{21,22}. In order to further investigate the shear dynamo problem, several other analytical frameworks have been reported^{23–25}. Along with these analytical attempts, it has been reported, based on direct numerical simulation that a driven small-scale, purely non-helical turbulence enhances the exponential growth of large scale magnetic energy in the presence of non-rotating linear shear flows^{26–28}. For example, it is found that^{27,28}, the LSD growth rate scales linearly with the S (where S is the shear flow strength). On the other hand, using a kinematic dynamo model, it has been shown that, unlike a linear relationship, the dynamo growth rate scales as $S^{\frac{2}{3}}$ ²⁹.

It is clear from the preceding discussion that theoretical and computational efforts are being put to understand the origin of large-scale dynamo action. Numerical studies have also been carried out on the shear dynamo action for large scale velocity shear and helical forced turbulence³⁰ and provide an effective explanation for large-scale dynamo action using a propagating wave-like dynamo solution³⁰. The primary difficulty lies in controlling the fluctuations on a small scale, as the small scale magnetic fields are regarded to be harmful to the dynamo action on a larger scale³¹. In the presence of large-scale velocity shear and non-helical flows, recent work provides an evidence of large-scale magnetic field generation from small-scale dynamos^{31,32}. This intriguing numerical observation has been explained using the concept of “magnetic shear current effect”^{31–34}. The generation of large-scale magnetic fields is the primary focus of all of these studies.

An alternate school of thought for LSD is to decrease the efficiency of small scales rather than trying to increase the activity of large-scale dynamos^{35–37}. Kinematic dynamo model has been used to examine shear dynamo activity with superimposed large-scale shear flow and small-scale helical base flow^{35,36}. For the numerical experiment, a well-known time-dependent 2.5-dimensional GP flow³⁸ has been considered. The presence of symmetry along one spatial dimension in GP flow³⁸ allows one to effectively transform the three-dimensional (3D) kinematic dynamo problem into a two-dimensional (2D) one. The results of numerical simulation led to the conclusion that the interaction between large-scale shear flow and small-scale helical flow does not boost the induction process. Instead, it slows down the small-scale dynamo growth rate, which in turn makes it possible for the large-scale dynamo action to become apparent^{35–37}. This idea is sometimes referred to as the “suppression principle”. In addition, propagating dynamo waves¹ have been observed, which is a hallmark of large-scale dynamo activity^{35–37}. By taking magnetic feed back into consideration (non-linear dynamo action) this issue has been revisited^{39–41}.

Recently, the shear-dynamo activity in the non-helical limit has been investigated numerically using both the

kinematic and self-consistent (with magnetic feed back) dynamo models⁴². In addition to a linear shear, the model also incorporates a random non-helical white-noise as a body force. This model has also been used to explain why existence of large-scale velocity shear is a favourable condition for small-scale dynamos. The turbulence caused by flow shear provides an explanation for the enhancement of small-scale dynamo⁴².

In the context of shear dynamo problem, the effect of flow shear on non-helical base flow is studied sparsely. In this present work, we have investigated the shear dynamo action using a kinematic dynamo model. In our model, the velocity field is not simulated using the Navier-Stokes equation; instead, it is given and remains unchanged throughout the simulation. As a flow drive for our simulation, we have considered a recently reported three-dimensional Yoshida-Morrison flow (or YM flow⁴³ in short). One of the interesting features of YM flow is that, its mirror symmetry (kinetic helicity) can be controlled by varying the magnitude of certain flow parameter⁴⁴. In the maximal helicity limit, YM flow resembles the well-known Arnold-Beltrami-Childress (ABC) flow, while in the non-helical limit, it is known as EPI2D flow⁴³. The ABC flow, but not the EPI2D flow, is a well-known candidate for fast dynamo action. Here, we investigate the effect of flow shear on dynamo instability. For a helical base flow, such as ABC flow, the inductive process is known to result in an exponential increase in magnetic energy in the absence of shear flows. Our spectral analysis supports the notion that this dynamo operates on a relatively small scales. We have also identified that, for this helical base flow (ABC flow), the presence of flow shear effectively suppresses small-scale dynamo activity over a broad range of the magnetic Reynolds number R_m . Several authors^{35–37} have reported this suppression mechanism using a quasi-2D helical base flow (GP flow)³⁸ with a large scale shear. Here, we have observed similar suppression activity using a full 3D helical ABC flow.

The above said picture changes dramatically when EPI2D flow is considered as the base flow. We find that the EPI2D flow is unable to induce exponential amplification of magnetic energy in the absence of shear flows. Interestingly, when the shear flow is considered, the small scale EPI2D flow is found to generate exponentially growing magnetic energy with time. In other words, our numerical analysis suggests that, in the presence of shear flow, an otherwise non-dynamo producing non-helical base flow (EPI2D flow) can effectively generate fast dynamo activity. We also observe, through numerical simulation, that the strength of shear flows has a significant impact on the amount of small-scale dynamo activity. We have obtained a generalized algebraic (combination of linear and non-linear) scaling, for the growth rate of magnetic energy with shear flow strength S as $\gamma = -aS + bS^{\frac{2}{3}}$, where a and b are positive real constants. It is observed that, our numerical finding of depending of γ on S is in agreement with several earlier analytical works^{29,45} while generalizing the same. The robustness

of our numerical finding is tested using shear flows with varying shear length scales, in addition, for a number of different small-scale base flows. Accretion discs, galaxies, jets, stellar convective zones, and so on all include hydrodynamic flows that are characterized by significant flow shear, suggesting that the dynamo mechanisms under consideration may play a key role in the creation of magnetic fields in these astrophysical scenarios.

The organization of the paper is as follows. In Sec. II we present about the dynamic equations. Our numerical solver and simulation details are described in Sec. III. The initial conditions, parameter details are shown in Sec. IV. Section V is dedicated to the simulation results on induction dynamo action that we obtained from our code and finally the summary and conclusions are listed in Sec. VI.

II. GOVERNING EQUATIONS

The governing equations to study kinematic fast dynamo action for the single fluid MHD plasma are as follows,

$$\frac{\partial \vec{B}}{\partial t} + \vec{\nabla} \cdot (\vec{u} \otimes \vec{B} - \vec{B} \otimes \vec{u}) = \frac{1}{R_m} \nabla^2 \vec{B} \quad (1)$$

$$\vec{\nabla} \cdot \vec{B} = 0 \quad (2)$$

where, \vec{u} , \vec{B} and R_m represent the velocity, magnetic fields and magnetic Reynolds number respectively. The magnetic Reynolds number (R_m) is defined as, $R_m = \frac{u_0 L}{\eta}$, where η is magnetic diffusivity and u_0 is a typical velocity scale. Time is normalized to Alfvén times (i.e, time taken for an Alfvén wave to traverse the simulation domain) and length to a typical characteristic length scale L (here it is the length of simulation domain). The symbol “ \otimes ” represents the dyadic between two vector quantities.

For solving the above set of equations at high grid resolution, we have developed a suite of GPU codes namely GMHD3D, which is briefly described in the following Section.

III. SIMULATION DETAILS: GMHD3D SOLVER

In this Section, we discuss the details of the numerical solver along with the benchmarking of the solver carried out by us. In order to study the plasma dynamics governed by MHD equations described above, we have recently upgraded an already existing well benchmarked single GPU MHD solver⁴⁶, developed in house at Institute For Plasma Research to multi-node, multi-card (multi-GPU) architecture for better performance⁴⁷. This newly upgraded GPU based magnetohydrodynamic solver (*GMHD3D*) is now capable of handling very large grid sizes. *GMHD3D* is a multi-node, multi-card, three dimensional (3D), weakly compressible, pseudo-spectral,

visco-resistive solver⁴⁷. This suite (GMHD3D) includes both 2-dimensional and 3-dimensional HydroDynamic (HD) and MagnetoHydrodynamic (MHD) solvers. It uses pseudo-spectral technique to simulate the dynamics of 3D magnetohydrodynamic plasma in a cartesian box with periodic boundary condition. By this technique one calculates the spatial derivative to evaluate non-linear term in governing equations with a standard $\frac{2}{3}$ de-aliasing rule⁴⁸. OpenACC FFT library (AccFFT library⁴⁹) is used to perform Fourier transform and Adams-bashforth time solver, for time integration. For 3D iso-surface visualization, an open source Python based data converter to VTK (Visualization Tool kit) by “PyEVTK”⁵⁰ is developed, which converts ASCII data to VTK binary format. After dumping the state data files to VTK, an open source visualization softwares, VisIt 3.1.2⁵¹ and Paraview⁵² is used to visualize the data. For this present work, the new solver’s accuracy with the single GPU solver has been cross-checked and it is verified that the results match upto machine precision. Further, several other benchmarking studies have been performed such as, the 3D kinematic dynamo effect^{53–56}, have been reproduced with ABC flow at grid resolution 64^3 . Details of these are presented in Appendix A. As will be discussed in the coming Section, numerical simulations reported here are performed in 256^3 grid size.

As discussed in the Introduction, to study the kinematic fast dynamo action, an accurate selection of “drive” velocity field is crucial, which we discuss in the Section to follow.

IV. INITIAL CONDITION

Recently Yoshida and Morrison⁴³ (YM) proposed a new intermediate class of flow, which may be regarded as a topological bridge between quasi-2D and 3D flow classes. The flow is formulated as follows:

$$\vec{u}_b = u_0 \alpha \vec{u}_+ + u_0 \beta \vec{u}_- \quad (3)$$

with

$$\vec{u}_+ = \begin{bmatrix} B \sin(k_0 y) - C \cos(k_0 z) \\ 0 \\ A \sin(k_0 x) \end{bmatrix} \quad (4)$$

and

$$\vec{u}_- = \begin{bmatrix} 0 \\ C \sin(k_0 z) - A \cos(k_0 x) \\ -B \cos(k_0 y) \end{bmatrix} \quad (5)$$

so that,

$$\begin{aligned} u_x &= \alpha u_0 [B \sin(k_0 y) - C \cos(k_0 z)] \\ u_y &= \beta u_0 [C \sin(k_0 z) - A \cos(k_0 x)] \\ u_z &= u_0 [\alpha A \sin(k_0 x) - \beta B \cos(k_0 y)] \end{aligned} \quad (6)$$

where k_0 , α , β , A, B and C are arbitrary real constants. For the present study, we consider the value of u_0 , α , A,

B and C to be unity. In the present work, we consider Eq. 3 as our base flow \vec{u}_b . The variation of β value in YM flow leads to new classes of base flows.

For example, for $\beta = 0$, Yoshida et al.⁴³ classify this flow as EPI-2D flow which is given by :

$$\begin{aligned} u_x &= [\sin(k_0 y) - \cos(k_0 z)] \\ u_y &= 0 \\ u_z &= [\sin(k_0 x)] \end{aligned} \quad (7)$$

This flow (i.e, Eq. 7) is dependent on all the 3 spatial coordinates (i.e, x, y, z), whereas only two flow components are nonzero. Thus EPI-2D flow is quasi-2D in nature.

As can be expected, for $\beta = 1$ Eq. 6 becomes the well known Arnold–Beltrami–Childress flow [ABC] like flow,

$$\begin{aligned} u_x &= [\sin(k_0 y) - \cos(k_0 z)] \\ u_y &= [\sin(k_0 z) - \cos(k_0 x)] \\ u_z &= [\sin(k_0 x) - \cos(k_0 y)] \end{aligned} \quad (8)$$

As β is varied from 0 to 1.0, a whole set of intermediate class of flows emerge, such that a normalized fluid helicity is exactly 0.0 for $\beta = 0$ and is maximum for $\beta = 1.0$ (i.e, ABC-like flows)⁴⁴. The variation of β value clearly leads to two distinguishable class viz helical ($\beta > 0$) and non-helical ($\beta = 0$) class of base flows⁴⁴.

In the following, we begin our investigation by focusing on the most well-known type of helical flow such as ABC-like base flow with $k_0 = 8$ and $\beta = 1$ (See Fig. 1a). In order to investigate the role of shear flows in the context of dynamo action, we introduce a periodic, large-scale shear flow (Eq. 9) (See Fig. 1b) of the form

$$\vec{u}_s = (0, S \cos(k_s x), 0) \quad (9)$$

where S is shear flow strength and k_s is the length scale of shear flow such that $k_s < k_0$. Hence we refer to the base flow i.e, the $\beta = 1$ ABC flow with mode number k_0 as small-scale flow and the flow with $k_s < k_0$ as large scale shear flow.

A recent work⁴⁴ has shown that a purely non-helical quasi-2-dimensional EPI2D flow alone is incapable of producing fast dynamo action due to insufficient stretching capability. In the context of dynamo activity, it is interesting to examine the effect of large-scale shear flows on non-helical base flows i.e, EPI2D flow. Hence, we consider a small scale ($k_0 = 8$) EPI2D flow along with a periodic large scale ($k_s = 1$) shear flow (Eq. 9) as our starting point (See Fig. 1c) to explore the shear dynamo action. In order to examine the robustness of our numerical findings, we have also considered a broken jet (two jets with opposed directions i.e., broken jets whose width is $\frac{\pi}{16}$ in a system of length 2π , placed alternately one after the other.) flow shear profile^{57–59} instead of a periodic shear profile ($k_s \rightarrow \infty$) (See Fig. 1d) to investigate the shear dynamo activity. Few additional studies with smaller scales ($k_0 = 16$) base flow have been performed

[Details of which are added in Supplementary information].

An initial value problem involving the induction equation for \vec{B} is solved for the prescribed flows $\vec{u} = \vec{u}_b + \vec{u}_s$ (See Eq. 3 & 9). We have considered a random perturbation as a seed initial magnetic field for our numerical experiments. We have also performed numerical experiments with a periodic initial magnetic field⁴ and a uniform magnetic field, and we find that the characteristics of the dynamo are largely insensitive to the initial conditions in both cases. For the rest of the discussion, we present results from random perturbations as initial magnetic field.

A. Parameter Details

We evolve the set of equations discussed in Section II, for class of YM flow profile, in a triply periodic box of length $L_x = L_y = L_z = 2\pi$ with time stepping (dt) = 10^{-4} and grid resolution 256^3 . We have also conducted grid size and time step size scaling studies (not shown) and find that values indicated above are adequate. With these initial conditions and parameter spaces we present our numerical simulation results.

V. SIMULATION RESULTS

The helical nature, chaotic property, and stretching ability of the ABC-like flow are known to be the primary causes for the generation of dynamo action^{44,53–56}.

In this study, we use a kinematic dynamo model and begin with a small scale ($k_0 = 8.0$) ABC-like flow (or YM flow with $\beta = 1.0$) to initiate our numerical experiment (See Fig. 1a). We perform our numerical runs for a wide range of magnetic Reynolds number R_m and compute the growth rate ($\gamma = \frac{d}{dt}(\ln E_B(t))$) of magnetic energy ($E_B = \frac{1}{2} \int_V (B_x^2 + B_y^2 + B_z^2) dx dy dz$) at late times (eg. $t \sim 80$ to 90). For sufficiently large values of the magnetic Reynolds number R_m , it is clear from Fig. 2a that the growth rate of magnetic energy does not saturate with R_m , a hallmark of fast dynamo action. It is well-known that magnetic field lines can stretch, twist, and fold (abbreviated as STF)⁴ in a kinematic dynamo model with ABC-like as the base flow. It can be seen that the magnetic energy is concentrated on smaller scales, which can be compared to the length scale of the flow that is driving it (See Fig. 2b). We have computed the magnetic energy spectral density $|\hat{B}(k)|$ (such that $\int |\hat{B}(k, t)|^2 dk$ is the total energy at time t and $k = \sqrt{k_x^2 + k_y^2 + k_z^2}$). From our spectral analysis, we observe that the majority of the power is concentrated in higher modes (i.e., on smaller length scales) (See fig. 2c). To put it another way, the dynamo is essentially a small scale or fluctua-

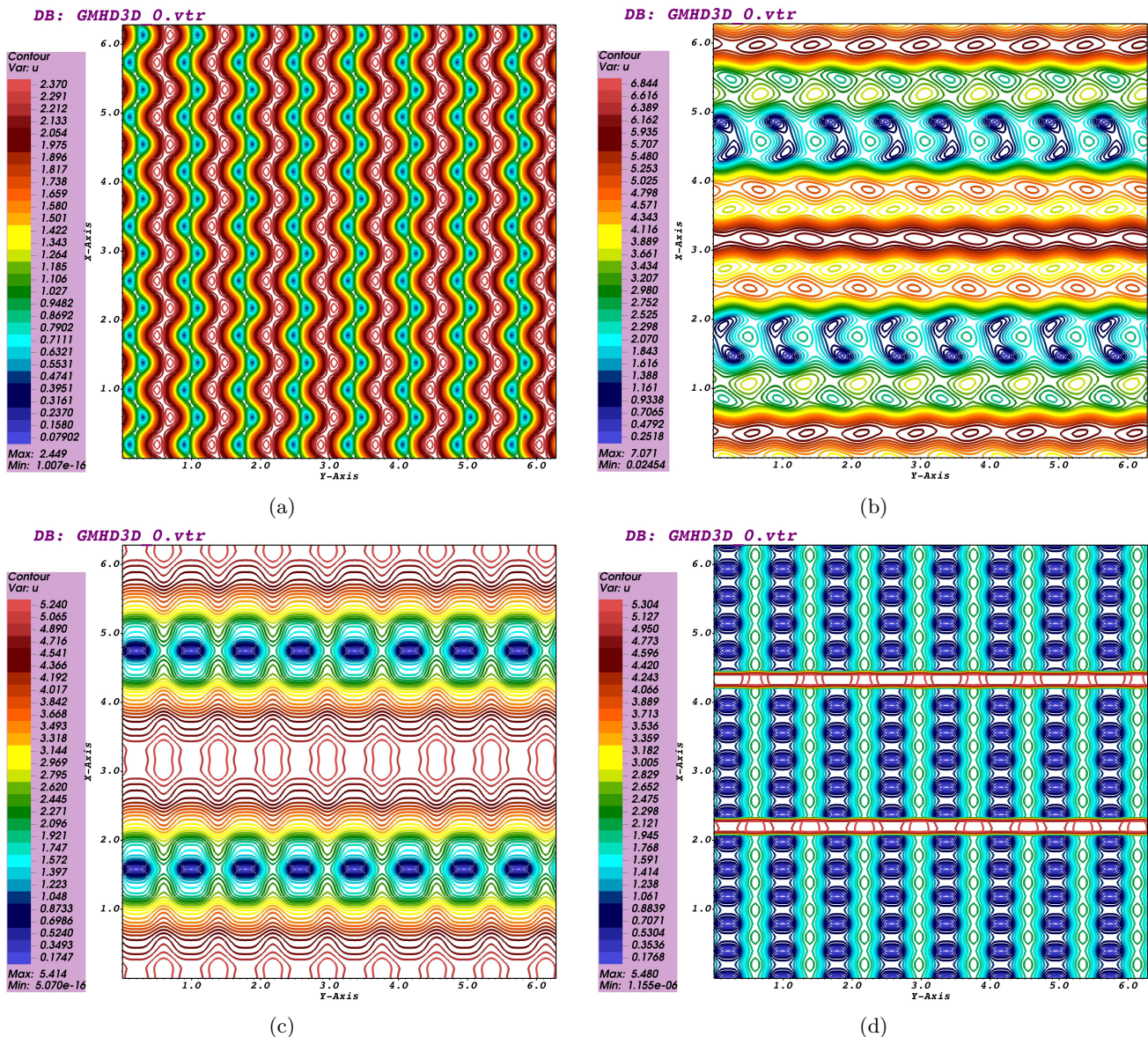


FIG. 1: Initial velocity ($u = \sqrt{u_x^2 + u_y^2 + u_z^2}$) profile in $X - Y$ plane for (a) small scale ($k_0 = 8$) helical ABC flow (b) superposition of small scale ($k_0 = 8$) helical ABC flow and large scale ($k_s = 1.0$) periodic shear (c) superposition of small scale ($k_0 = 8$) non-helical EPI2D flow and large scale ($k_s = 1$) periodic shear (d) superposition of small scale ($k_0 = 8$) non-helical EPI2D flow and broken jet (i.e $k_s \rightarrow \infty$) flow shear^{57–59} profile.

tion dynamo (SSD). Investigating the effect of flow shear on this highly helical and chaotic 3D ABC-like flow is an interesting line of inquiry.

Several authors^{30,35,36,60,61} have addressed the impact of large-scale shear on helical base flows in the context of dynamo action. In some of the earlier works have considered a circularly polarized, time dependent 2.5-dimensional base flow namely GP flow³⁸ as a driver for dynamo simulation. In essence, the time dependency of GP flow introduces the chaoticity and stretching property into the system, both of which are necessary for dynamo activity. Another important property of GP flow is that,

one can control its reflectional symmetry (helicity distribution) by varying certain physical parameter³⁵ similar to our β parameter in YM flow^{43,44}.

Here, using a kinematic dynamo model, we examine the impact of large scale ($k_s = 1$) flow shear (Eq. 9) on small-scale ($k_0 = 8$) 3-dimensional YM flow with $\beta = 1$ (i.e, ABC-like flow) (Eq. 8) (See Fig. 3). As part of our study, we have conducted numerical simulations with varying shear flow strengths S . As can be seen in Fig. 3, the small-scale dynamo action is suppressed by the large-scale ($k_s = 1$) shear flow. The magnetic energy growth rate is found to decrease over a broad range of magnetic

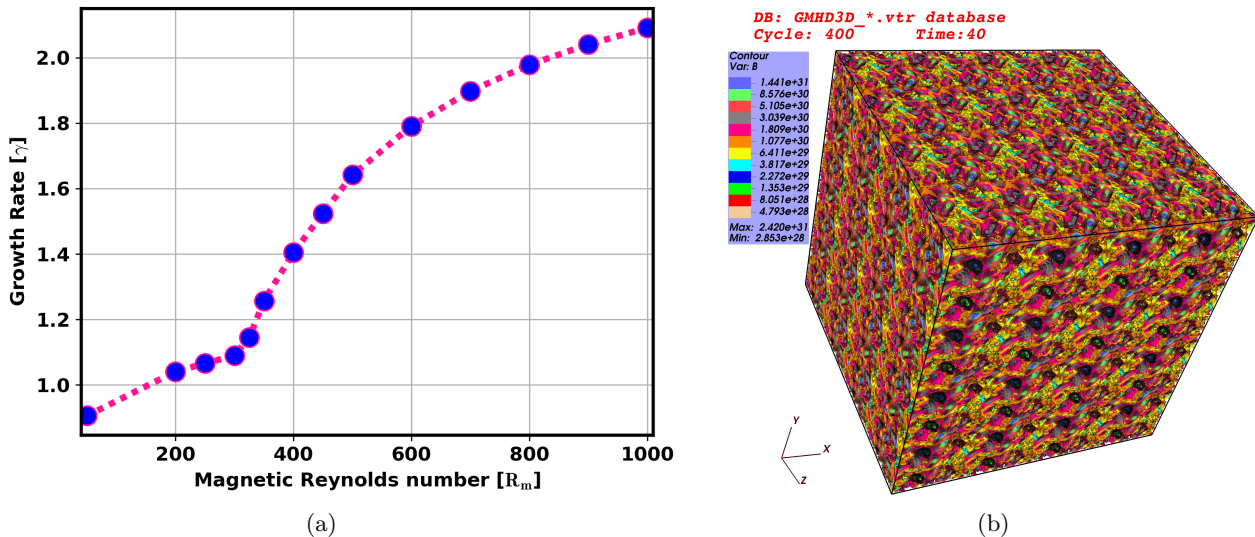


FIG. 2: (a) Magnetic energy ($E_B = \frac{1}{2} \int_V (B_x^2 + B_y^2 + B_z^2) dx dy dz$) growth rate ($\gamma = \frac{d}{dt} (\ln E_B(t))$) at late times (eg. $t \sim 80$ to 90) for small scale helical ABC-like flow in the absence of shear flow ($S = 0$). (b) Magnetic energy iso-surface in the absence of shear flow, $S = 0$ (magnetic energy is effectively dominated by small scales, hence a small scale dynamo (SSD)) [See **Movie1.mp4**]. (c) Calculation of magnetic energy spectral density (for $S = 0$ & 5) $|\hat{B}(k)|$ (such that $\int |\hat{B}(k, t)|^2 dk$ is the total energy at time t (inset view: in linear scale)). Simulation details: grid resolution 256^3 .

Reynolds numbers R_m . The interaction between helical base flows and large scale shear effectively limits the growth of small scales (i.e, fluctuations). A possible reason could be that in a fully chaotic system, two neighboring fluid elements would diverge exponentially in time. If one includes a regulating flow (shear flow), the two neighboring fluid elements will diverge, but algebraically - which implies less chaotic flow and hence reduced dynamo growth³⁶. The primary function of flow shear is to diminish the efficacy of fast dynamo action at small

scales, which in turn may be interpreted as the flow shear is effectively helping to boost the activity of dynamos at larger scales, or the mean field. This possibility is also reported by a number of authors^{35-37,62} in the past, for 2.5 dimensional helical GP flow. Hence our findings in $\beta = 1$ limit of YM flow which corroborate with earlier work on helical flows, may be regarded as a benchmark for GMHD3D solver. In light of this background, a reasonable question to ask is the following: what kind of effect does shear flows have on a small-scale base flow

that is not helical and does the scale of flow shear matter at all?

To address this, we employ direct numerical simulation (DNS) to examine the effect of a superposition of large-scale shear and purely non-helical short-scale EPI2D flow (See Fig. 1c). When there is no flow shear present, the dynamo effect is absent for an EPI2D flow. The magnetic energy growth rate ($\gamma = \frac{d}{dt}(\ln E_B(t))$) for small scale EPI2D flow in the absence of flow shear, is negative over a wide range of magnetic Reynolds numbers R_m (See Fig. 4a for $S = 0$). This is an obvious indication of non-dynamo activity. However, Zeldovich's classic anti-dynamo theorem provides an alternative explanation for this^{3,63}. When this small-scale, non-dynamo-producing, EPI2D flow is superposed with a large-scale flow shear, the dynamics is found to undergo an interesting transformation. We have carried out our numerical experiments across a broad range of shear flow strengths (S) and magnetic Reynolds numbers (R_m) (See Fig. 4a for $S = 1$ to 20). In the presence of a non-zero shear flow strength, as shown in Fig. 4a, magnetic energy growth is clearly visible. At sufficiently high magnetic Reynolds numbers R_m , the growth rate of magnetic energy (γ) continues to vary significantly and is found not to saturate with R_m , verifying one of the defining features of fast dynamo action^{4,56}. We have calculated $\frac{d\gamma}{dR_m}$ as a function of R_m and find that the value of $\frac{d\gamma}{dR_m}$ to be slowly varying, even at the maximum magnetic Reynolds number [See Fig. 4b].

We have visualized the iso-surfaces of the magnetic fields (Iso-B surfaces) in three dimensions and find that the magnetic energy is concentrated in two bands near the segments with strong velocity gradients (See Fig. 5). Magnetic energy iso-surfaces are dominated by small-scale structures (compared to the length scale of the flow), as is evident from Fig. 5. We have computed the magnetic energy spectral density $|\hat{B}(k)|$ (such that $\int |\hat{B}(k, t)|^2 dk$ is the total energy at time t and $k = \sqrt{k_x^2 + k_y^2 + k_z^2}$) to verify our findings. It is seen from Fig. 4c that the most of the magnetic energy is at the higher mode numbers (shorter length scales). To further illustrate our point, we have plotted the magnetic energy spectral density over time for each of the modes (eg. $|\hat{B}(k = 1), t|$, $|\hat{B}(k = 20), t|$, $|\hat{B}(k = 30), t|$, $|\hat{B}(k = 50), t|$, $|\hat{B}(k = 70), t|$ etc.). It is easy to see from Fig. 4d that the higher modes (shorter length scales) contain higher energies; this is a primary characteristic of SSD.

In addition, we plot the rate of increase in magnetic energy (γ) as a function of the shear flow strength (S) for non-helical base flow. Figure 6 demonstrates unambiguously that as the amplitude of the shear flow increases, the rate of growth of magnetic energy also increases. Spectral analysis confirms the SSD-like structure for a given value of shear flow strength (S) (See Fig. 4c). Based on the evidence presented in Fig. 6, we conclude that the effect of large-scale shear flows in this instance is not to suppress the SSD activity, but rather to amplify

it. Additionally, we obtain a generalized algebraic (combination of linear and non-linear) scaling (based on χ^2 minimization) for the rate of increase of magnetic energy (γ) in the form $\gamma(S) = -aS + bS^{\frac{2}{3}}$ (See Fig. 6), where a & b are real fit coefficients. Our numerical finding of dependency of γ on S is found to be in close agreement with analytic predictions^{29,45}. It is observed that, for a given random smooth velocity field, large-scale shear can support a small scale dynamo (SSD) with a scaling of $S^{\frac{2}{3}}$ ⁴⁵, which is consistent with an upper bound for growth rates anticipated afterward²⁹.

It has been recently proposed⁴² that, a random non-helically driven, dissipative model can enhance SSD action. This work reports on amplification of SSD using a kinematic dynamo model which solves a Navier-Stokes equation for the fluid flow, along with a linear background shear and a random non-helical white noise drive⁴². In yet another model, the shear is self-consistently driven by the presence of an in-plane temperature gradient resulting in SSD⁶⁴.

In contrast to these earlier studies, in our model we have imposed a driven shear velocity field with a three-dimensional flow field (the helicity of which can be controlled) and studied the growth of magnetic energy by only evolving the induction equation for magnetic fields in a triply periodic three-dimensional box (i.e, the velocity field is not evolved using the Navier-Stokes equation; rather, it is given and remains static throughout the simulation.). Using this configuration, we have demonstrated unambiguously how flow shears enhance small scale dynamo (SSD) activity for non-helical base flows.

A natural question is whether the dynamo property found here is associated to the scale of the shear flow profile. To answer this question, we have conducted numerical experiments using broken jet flow shear as an extreme case (i.e, $k_s \rightarrow \infty$ or, $k_s \sim k_{max}$ numerically speaking) (See Fig. 1d). This shear profile appears frequently in hydrodynamics studies, especially those used to investigate Navier-Stokes turbulence⁵⁷⁻⁵⁹. EPI2D flow is shown to generate magnetic energy ($E_B = \frac{1}{2} \int_V (B_x^2 + B_y^2 + B_z^2) dx dy dz$) in an exponential fashion in the presence of broken jet flow (with $k_s \sim k_{max}$) shear. Furthermore, from Fig. 7a, it is clear that with increase in magnetic Reynolds number R_m , the growth rate of magnetic energy ($\gamma = \frac{d}{dt}(\ln E_B(t))$) is found not to reach a saturation point in line with what is expected for a fast dynamo action. With the help of an iso-surface representation of magnetic energy (See Fig.8), we are able to determine that the generated magnetic energy is mostly contained in smaller scales (compared to the length scale of the flow that is driving it), making the dynamo a small-scale dynamo (SSD). In addition, we have estimated the magnetic energy spectral density associated with each mode, such as $|\hat{B}(k = 1), t|$, $|\hat{B}(k = 20), t|$, $|\hat{B}(k = 30), t|$ etc., and monitor its time-dependent evolution. As was the case in the previous example, it is found that the energy is concentrated in higher modes or shorter length scales (See Fig. 7b); consequently, the dynamo can be thought

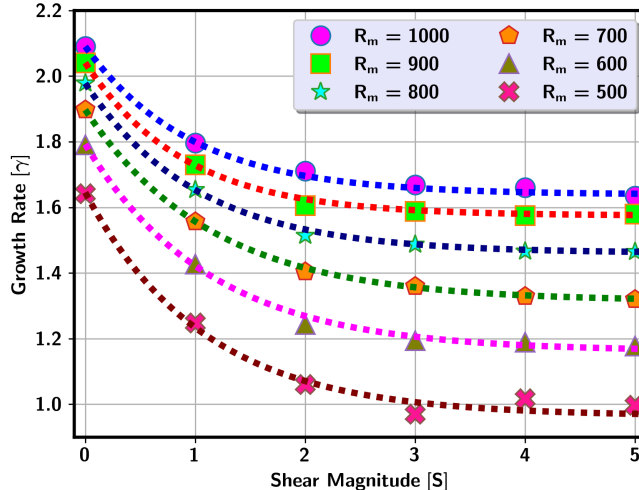


FIG. 3: Magnetic energy ($E_B = \frac{1}{2} \int_V (B_x^2 + B_y^2 + B_z^2) dx dy dz$) growth rate ($\gamma = \frac{d}{dt}(\ln E_B(t))$) as function of shear flow strength (S) for a helical base flow (ABC-like (i.e, $\beta = 1.0$) flow). As the shear strength (S) increases, small scale magnetic energy growth rate decreases. The profile of magnetic energy iso-surface (for $S = 0$) and magnetic energy spectral density (for $S = 0$ & $S = 5$) are shown in Fig. 2

of as a small-scale dynamo (SSD). We also plot the magnetic energy growth rate ($\gamma = \frac{d}{dt}(\ln E_B(t))$) as a function of shear flow strength (S), and we obtain the same generalized algebraic scaling $\gamma(S) = -aS + bS^{\frac{2}{3}}$ (based on χ^2 minimization), where a & b are real fit coefficients as obtained for broken jet shear flow (See Fig. 7c). Hence, in the presence of broken jet flow shear^{57–59} as well, our numerical observation unambiguously demonstrates that there is an onset and increase in the activity of small scale dynamo (SSD). As the effect is found to be robust at largest and smallest shear scale lengths, we conclude that the scaling of $\gamma(S)$ vs S appears to be independent of shear flow scale (except that the real coefficients a and b are to be determined accordingly) and robust.

To further convince ourselves regarding the generality of our finding, we have considered yet another non-helical flow namely Taylor-Green (TG) flow and investigate the effect of flow shear on the dynamo activity with TG flow as the base flow. It is found that the fundamental observations remain unaltered (See Supplementary information for details).

VI. SUMMARY AND CONCLUSION

In this work, we have performed direct numerical simulations (DNS) of kinematic dynamos using a 3-dimensional magnetohydrodynamic model at modest grid resolutions. By considering a simple kinematic dynamo model, we are able to demonstrate that the small-scale helical YM flow with $\beta = 1.0$ (ABC-like flow) generates rapid dynamo action over a broad range of magnetic Reynolds number. The results of our spectral

calculation demonstrate without a doubt that the fully developed dynamo is, in effect, a small scale dynamo (SSD). In addition, it has been shown that the presence of a flow shear reduces the efficiency of small-scale dynamo action. This interesting finding appears to be consistent with several earlier works reported for a 2.5-dimensional GP flow, which may also be considered as a good benchmark for GMHD3D solver.

Our major findings are:

- A non-dynamo producing, small scale non-helical EPI2D flow shows fast SSD activity when flow shear is introduced. More importantly, unlike fully helical flows, it has been observed that, for EPI2D non-helical flows, the small-scale dynamo action (SSD) increases as the shear flow strength (S) increases. The spectral diagnostics also are found to be in agreement with the observation.
- A generalized algebraic scaling for the magnetic energy growth rate (γ) as a function of the shear flow strength (S) has been obtained. Our numerical observation is supported by a number of recent analytical works^{29,45}.
- We have performed our numerical experiments using broken jet flow ($k_s \rightarrow \infty$. i.e, $k_s \sim k_{max}$ numerically speaking) shear profile, and we have found that the primary findings are unaffected. The mechanism of onset of dynamo from non-helical base flows in the presence of shear flows is found to be independent of the scale of shear flows.
- The scaling of $\gamma(S) = -aS + bS^{\frac{2}{3}}$, where a & b are real fit coefficients is found to be robust and not dependent on shear flow length scale k_s .

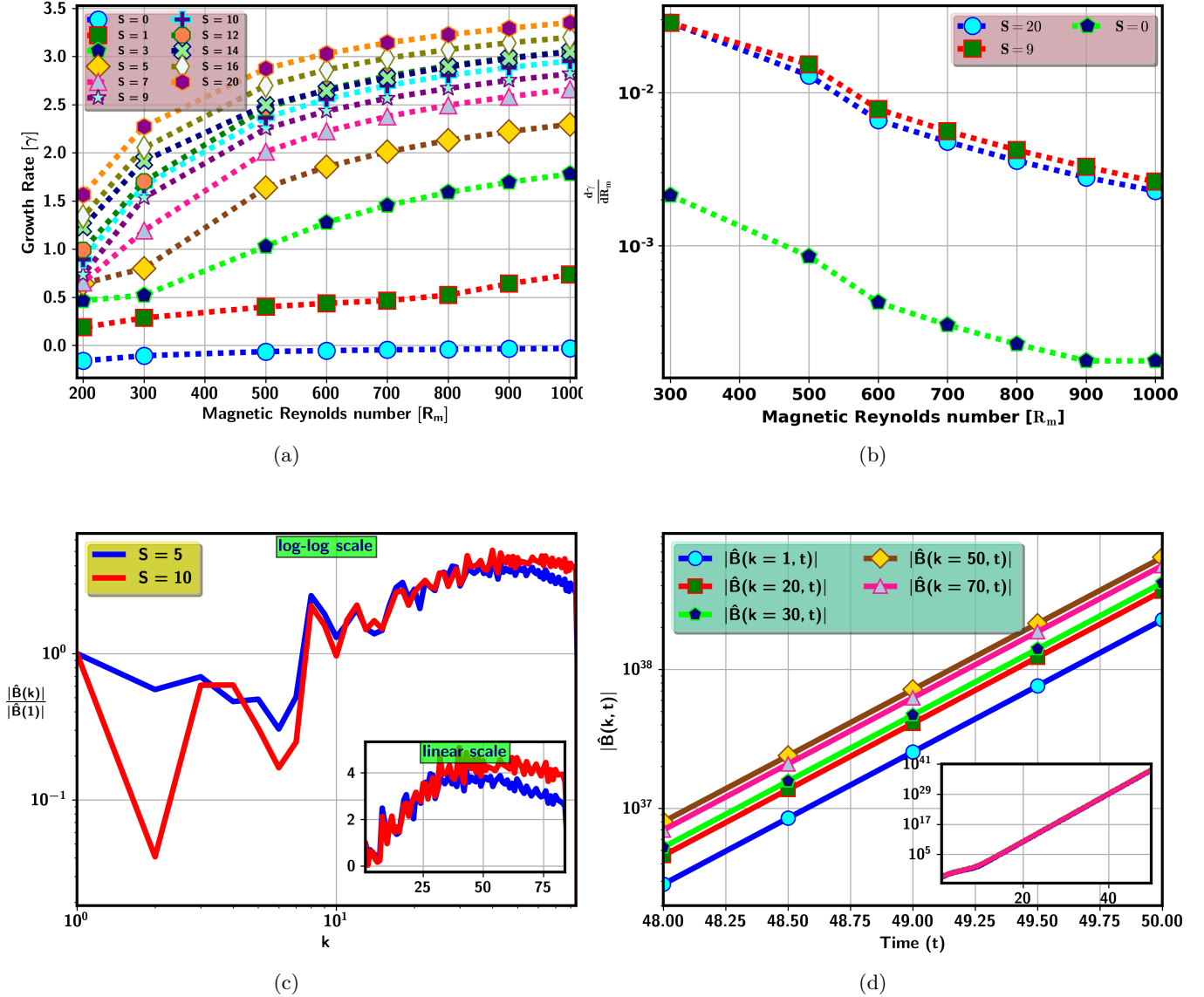


FIG. 4: (a) Magnetic energy ($E_B = \frac{1}{2} \int_V (B_x^2 + B_y^2 + B_z^2) dx dy dz$) growth rate ($\gamma = \frac{d}{dt} (\ln E_B(t))$) at late times (eg. $t \sim 80$ to 90) as a function of magnetic Reynolds number R_m for small scale ($k_0 = 8$) non-helical EPI2D flow and for various values of S , the large scale ($k_s = 1$) periodic shear flow strength. (b) Calculation of $\frac{d\gamma}{dR_m}$ as a function of magnetic Reynolds number (R_m) for different values of shear flow strength S . (c) Calculation of magnetic energy spectral density $|\hat{B}(k)|$ (such that $\int |\hat{B}(k, t)|^2 dk$ is the total energy at time t) for two different values of shear flow strength S , namely $S = 5$ and $S = 10$ (inset view: in linear scale). (d) Time evolution of magnetic energy spectral density contained in each mode. The higher mode numbers (shorter length scales) contain higher energies at all later times shown; which is a primary characteristic of small scale dynamo (SSD).

- We have also carried out the same analysis for a different well-known non-helical base flow, known as the Taylor-Green flow, and found that our results remain valid (See Supplementary information for details). Our numerical findings are basically found to be robust.

To conclude, we have investigated the effect of shear flows on the onset of dynamo instability on non-helical

base flows, using a modest resolution and a wide range of magnetic Reynolds numbers and for flow shear scale lengths. Our numerical analysis reveals that the small-scale dynamo action is suppressed by flow shear for base helical flows, but is amplified for base non-helical flows. We also believe these dynamos should play an important role in a wide variety of astrophysical ob-

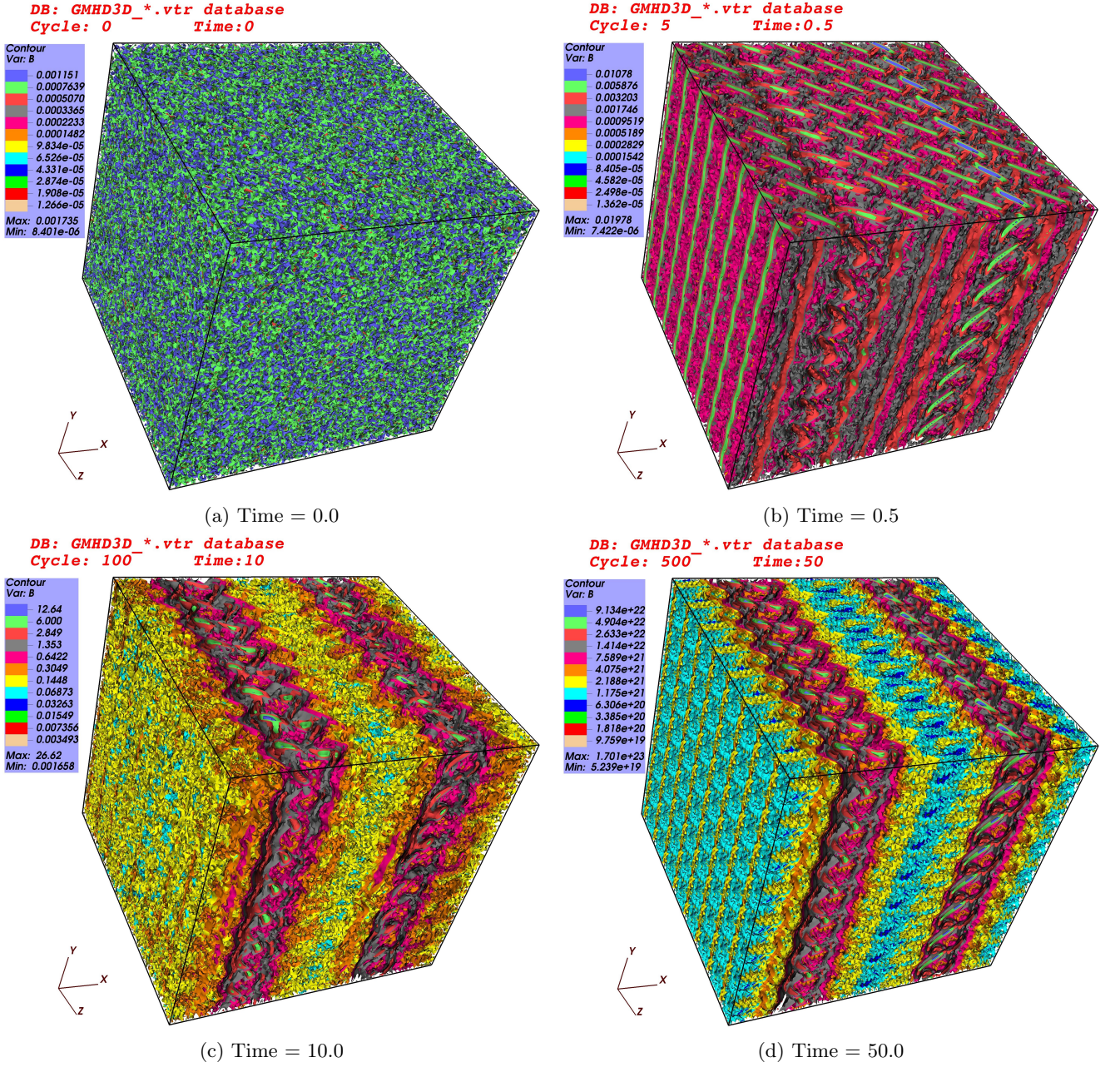


FIG. 5: Time evolution of 3-dimensional magnetic field iso-surfaces (Iso-B surfaces) for a given small scale ($k_0 = 8$) EPI2D flow and large scale ($k_s = 1$) periodic shear. Dominant magnetic energies are mostly confined in two regimes restricted near the segments ($z = \frac{\pi}{2}$ and $z = \frac{3\pi}{2}$) where the velocity gradients are strongest. The structures are mostly dominated by small scale structures (SSD) [Movie2.mp4]. Simulation details: grid resolution 256^3 , shear flow strength $S = 5.0$, magnetic Reynolds number $R_m = 200.0$. Visualization in log scale.

jects, especially in highly symmetric regions like the mid plane of accretion disks where flow shear is known to be substantial^{65,66}. However, it may be argued that in actual astrophysical conditions, the magnetic back reaction on the velocity field cannot be disregarded. Unlike the scenario presented above, velocity fields in such situations are not predetermined. We hope to address several of these issues in a future communication.

VII. ACKNOWLEDGMENTS

The simulations and visualizations presented here are performed on GPU nodes and visualization nodes of Antya cluster at the Institute for Plasma Research (IPR), INDIA. One of the author S.B is thankful to Dr. Rupak Mukherjee at Central University of Sikkim (CUS), Gangtok, Sikkim, India for providing an initial version

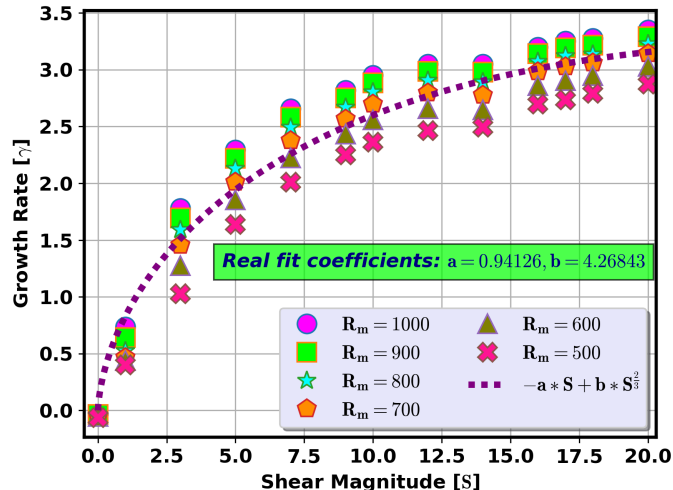


FIG. 6: Magnetic energy ($E_B = \frac{1}{2} \int_V (B_x^2 + B_y^2 + B_z^2) dx dy dz$) growth rate ($\gamma = \frac{d}{dt} (\ln E_B(t))$) as function of shear flow strength (S) for small scale ($k_0 = 8$) non-helical EPI2D flow and large scale ($k_s = 1$) periodic shear flow. As the shear strength (S) increases, small scale magnetic energy growth rate also increases following an algebraic scaling of the form $-aS + bS^{\frac{2}{3}}$ with $a = 0.94126$, $b = 4.26843$.

of *GMHD3D* code. S.B thanks N. Vydyanathan, Bengaluru and B. K. Sharma at NVIDIA, Bengaluru, India, for extending their help with basic GPU methods. S.B is grateful to Mr. Soumen De Karmakar at IPR, India for many helpful discussions regarding GPUs, and HPC support team of IPR for extending their help related to ANTYA cluster.

VIII. DATA AVAILABILITY

The data underlying this article will be shared on reasonable request to the corresponding author.

IX. CONFLICT OF INTEREST

The authors have no conflicts to disclose.

X. SUPPORTING INFORMATION

The following movies:

- [Movie1.mp4](#)
- [Movie2.mp4](#)
- [Movie3.mp4](#)

are added as integral multimedia files.

-
- [1] E. N. Parker, *Astrophys. J.* **122**, 293 (1955).
 [2] E. Parker, *Cosmical Magnetic Fields*, Clarendon (Oxford, 1979).
 [3] F. Rincon, *Journal of Plasma Physics* **85**, 205850401 (2019).
 [4] S. Childress and A. D. Gilbert, *Stretch, twist, fold: the fast dynamo*, vol. 37 (Springer Science & Business Media, 1995).
 [5] S. M. TOBIAS and F. CATTANEO, *Journal of Fluid Mechanics* **601**, 101–122 (2008).
 [6] G. K. Batchelor, *Proceedings of the Royal Society of London. Series A. Mathematical and Physical Sciences* **201**, 405 (1950).
 [7] A. Kazantsev, *Sov. Phys. JETP* **26**, 1031 (1968).
 [8] Y. B. Zel'Dovich, A. A. Ruzmaikin, S. A. Molchanov, and D. D. Sokoloff, *Journal of Fluid Mechanics* **144**, 1–11 (1984).
 [9] M. Meneguzzi, U. Frisch, and A. Pouquet, *Phys. Rev. Lett.* **47**, 1060 (1981), URL <https://link.aps.org/doi/10.1103/PhysRevLett.47.1060>.
 [10] A. A. Schekochihin, S. C. Cowley, S. F. Taylor, J. L. Maron, and J. C. McWilliams, *The Astrophysical Journal* **612**, 276 (2004), URL <https://dx.doi.org/10.1086/422547>.

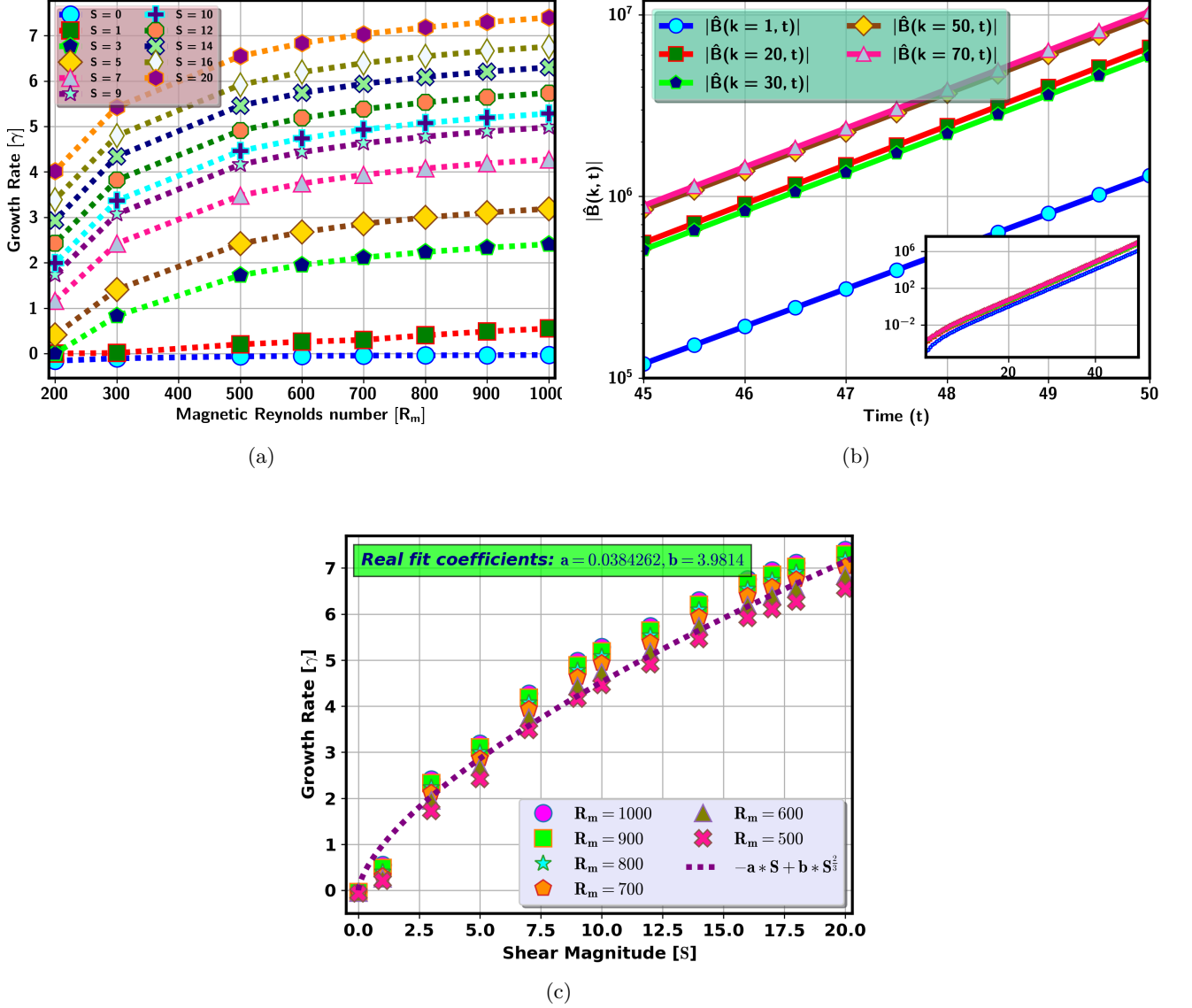


FIG. 7: (a) Magnetic energy ($E_B = \frac{1}{2} \int_V (B_x^2 + B_y^2 + B_z^2) dx dy dz$) growth rate ($\gamma = \frac{d}{dt} (\ln E_B(t))$) at late times (eg. $t \sim 80$ to 90) as a function of magnetic Reynolds number R_m for small scale ($k_0 = 8$) non-helical EPI2D flow and broken jet flow shear ($k_s \rightarrow \infty$. i.e. $k_s \sim k_{max}$ numerically speaking). (b) Time evolution of magnetic energy spectral density ($|\hat{B}(k, t)|$) contained in each mode. (c) Magnetic energy ($E_B = \frac{1}{2} \int_V (B_x^2 + B_y^2 + B_z^2) dx dy dz$) growth rate ($\gamma = \frac{d}{dt} (\ln E_B(t))$) as function of shear flow strength (S) for small scale ($k_0 = 8$) non-helical EPI2D flow and broken jet flow shear ($k_s \rightarrow \infty$). As the shear strength (S) increases, small scale magnetic energy growth rate also increases following an algebraic scaling of the form $-aS + bS^{2/3}$, with $a = 0.0384262$, $b = 3.9814$.

[11] V. Skoutnev, J. Squire, and A. Bhattacharjee, *The Astrophysical Journal* **906**, 61 (2021), URL <https://dx.doi.org/10.3847/1538-4357/abc8ee>.
 [12] V. Skoutnev, J. Squire, and A. Bhattacharjee, *Monthly Notices of the Royal Astronomical Society* **517**, 526 (2022), ISSN 0035-8711, <https://academic.oup.com/mnras/article-pdf/517/1/526/46356017/stac2676.pdf>, URL <https://doi.org/10.1093/mnras/stac2676>.

[13] M. Stix, *The Sun: an introduction* (Springer Science & Business Media, 2004).
 [14] H. K. Moffatt, *Magnetic field generation in electrically conducting fluids* (1978).
 [15] R. Monchaux, M. Berhanu, M. Bourgoin, M. Moulin, P. Odier, J.-F. Pinton, R. Volk, S. Fauve, N. Mor-dant, F. Pétrélis, et al., *Phys. Rev. Lett.* **98**, 044502 (2007), URL <https://link.aps.org/doi/10.1103/PhysRevLett.98.044502>.

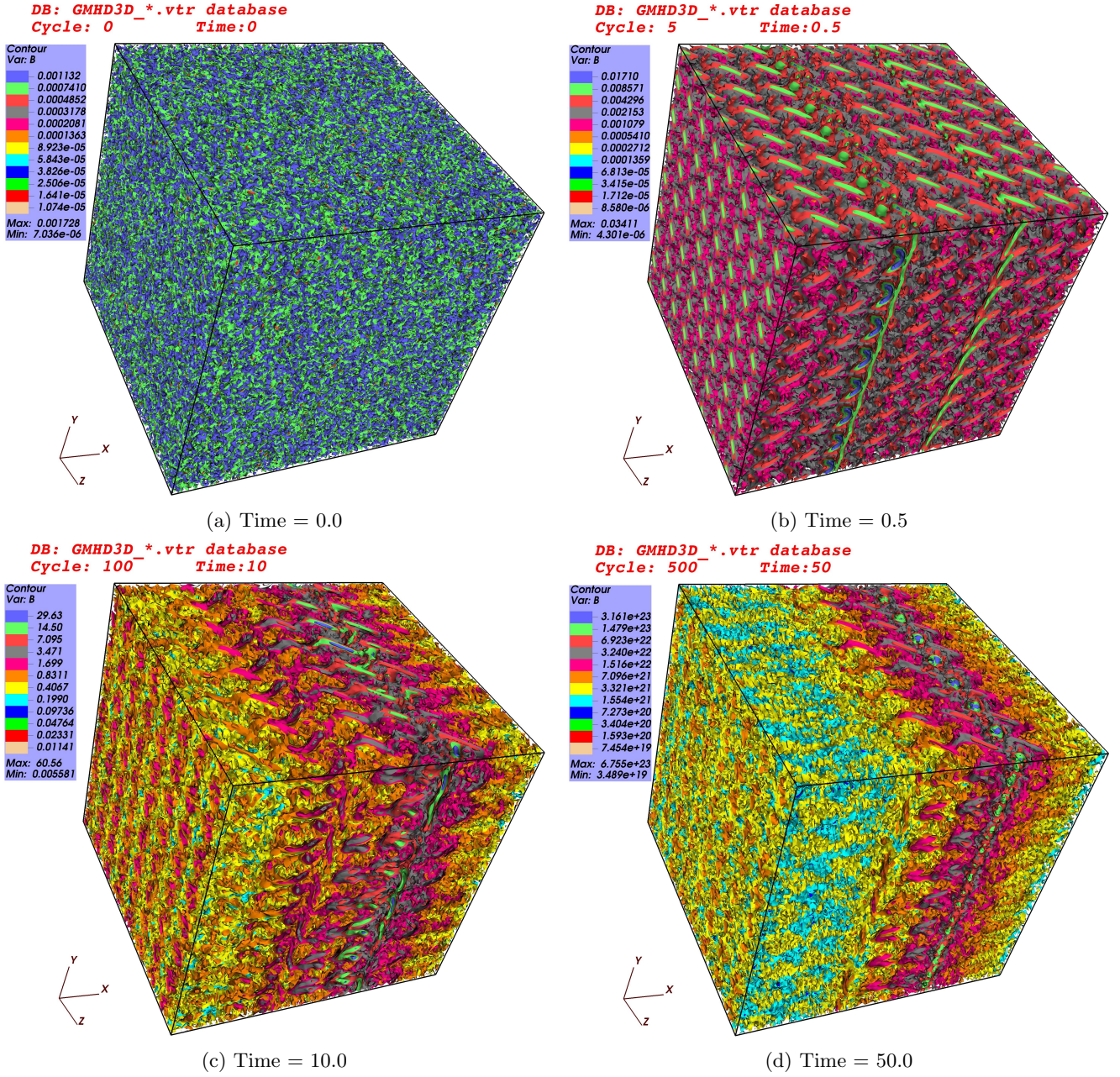


FIG. 8: Time evolution of 3-dimensional magnetic field iso-surfaces (Iso-B surfaces) for a given small scale EPI2D flow ($k_0 = 8$) and broken jet flow shear ($k_s \rightarrow \infty$. i.e. $k_s \sim k_{max}$ numerically speaking). The structures are mostly dominated by short scale structures (SSD) [Movie3.mp4]. Simulation details: grid resolution 256^3 , stepping time $dt = 10^{-4}$, shear flow strength $S = 5.0$, magnetic Reynolds number $R_m = 200.0$. Visualization in log scale.

- [16] Käpylä, P. J., Korpi, M. J., and Brandenburg, A., *A&A* **491**, 353 (2008), URL <https://doi.org/10.1051/0004-6361:200810307>.
- [17] D. W. Hughes and M. R. E. Proctor, *Phys. Rev. Lett.* **102**, 044501 (2009), URL <https://link.aps.org/doi/10.1103/PhysRevLett.102.044501>.
- [18] P. J. Käpylä, M. J. Korpi, and A. Brandenburg, *Monthly Notices of the Royal Astronomical Society* **402**, 1458 (2010), ISSN 0035-8711, <https://academic.oup.com/mnras/article-pdf/402/3/1458/3112103/mnras0402-1458.pdf>, URL <https://doi.org/10.1111/j.1365-2966.2009.16004.x>.
- [19] D. W. Hughes and M. R. E. Proctor, *Journal of Fluid Mechanics* **717**, 395–416 (2013).
- [20] F. CATTANEO and D. W. HUGHES, *Journal of Fluid Mechanics* **553**, 401–418 (2006).
- [21] S. Sridhar and K. Subramanian, *Phys. Rev. E* **79**, 045305 (2009), URL <https://link.aps.org/doi/10.1103/PhysRevE.79.045305>.

- [22] S. Sridhar and K. Subramanian, *Phys. Rev. E* **80**, 066315 (2009), URL <https://link.aps.org/doi/10.1103/PhysRevE.80.066315>.
- [23] S. SRIDHAR and N. K. SINGH, *Journal of Fluid Mechanics* **664**, 265–285 (2010).
- [24] S. Sridhar and N. K. Singh, *Monthly Notices of the Royal Astronomical Society* **445**, 3770 (2014), ISSN 0035-8711, <https://academic.oup.com/mnras/article-pdf/445/4/3770/6083514/stu1981.pdf>, URL <https://doi.org/10.1093/mnras/stu1981>.
- [25] N. K. Singh and S. Sridhar, *Phys. Rev. E* **83**, 056309 (2011), URL <https://link.aps.org/doi/10.1103/PhysRevE.83.056309>.
- [26] A. Brandenburg, K.-H. Rädler, M. Rheinhardt, and P. J. Käpylä, *The Astrophysical Journal* **676**, 740 (2008), URL <https://dx.doi.org/10.1086/527373>.
- [27] T. A. Yousef, T. Heinemann, A. A. Schekochihin, N. Kleeorin, I. Rogachevskii, A. B. Iskakov, S. C. Cowley, and J. C. McWilliams, *Phys. Rev. Lett.* **100**, 184501 (2008), URL <https://link.aps.org/doi/10.1103/PhysRevLett.100.184501>.
- [28] T. A. Yousef, T. Heinemann, F. Rincon, A. A. Schekochihin, N. Kleeorin, I. Rogachevskii, S. C. Cowley, and J. C. McWilliams, *Astronomische Nachrichten* **329**, 737 (2008), <https://onlinelibrary.wiley.com/doi/pdf/10.1002/asna.200811018>, URL <https://onlinelibrary.wiley.com/doi/abs/10.1002/asna.200811018>.
- [29] M. R. E. Proctor, *Journal of Fluid Mechanics* **697**, 504–510 (2012).
- [30] P. J. Käpylä and A. Brandenburg, *The Astrophysical Journal* **699**, 1059 (2009), URL <https://dx.doi.org/10.1088/0004-637X/699/2/1059>.
- [31] J. Squire and A. Bhattacharjee, *Phys. Rev. Lett.* **115**, 175003 (2015), URL <https://link.aps.org/doi/10.1103/PhysRevLett.115.175003>.
- [32] J. Squire and A. Bhattacharjee, *The Astrophysical Journal* **813**, 52 (2015), URL <https://dx.doi.org/10.1088/0004-637X/813/1/52>.
- [33] I. Rogachevskii and N. Kleeorin, *Phys. Rev. E* **68**, 036301 (2003), URL <https://link.aps.org/doi/10.1103/PhysRevE.68.036301>.
- [34] I. Rogachevskii and N. Kleeorin, *Phys. Rev. E* **70**, 046310 (2004), URL <https://link.aps.org/doi/10.1103/PhysRevE.70.046310>.
- [35] S. M. Tobias and F. Cattaneo, *Nature* **497**, 463 (2013).
- [36] F. Cattaneo and S. M. Tobias, *The Astrophysical Journal* **789**, 70 (2014), URL <https://dx.doi.org/10.1088/0004-637X/789/1/70>.
- [37] G. Nigro, P. Pongkitiwanchakul, F. Cattaneo, and S. M. Tobias, *Monthly Notices of the Royal Astronomical Society: Letters* **464**, L119 (2016), ISSN 1745-3925, <https://academic.oup.com/mnrasl/article-pdf/464/1/L119/9405140/slw190.pdf>, URL <https://doi.org/10.1093/mnrasl/slw190>.
- [38] D. J. Galloway and M. R. Proctor, *Nature* **356**, 691 (1992).
- [39] P. Pongkitiwanchakul, G. Nigro, F. Cattaneo, and S. M. Tobias, *The Astrophysical Journal* **825**, 23 (2016), URL <https://dx.doi.org/10.3847/0004-637X/825/1/23>.
- [40] R. J. Teed and M. R. E. Proctor, *Monthly Notices of the Royal Astronomical Society* **458**, 2885 (2016), ISSN 0035-8711, <https://academic.oup.com/mnras/article-pdf/458/3/2885/8006976/stw490.pdf>, URL <https://doi.org/10.1093/mnras/stw490>.
- [41] R. J. Teed and M. R. E. Proctor, *Monthly Notices of the Royal Astronomical Society* **467**, 4858 (2017), ISSN 0035-8711, <https://academic.oup.com/mnras/article-pdf/467/4/4858/11042356/stx421.pdf>, URL <https://doi.org/10.1093/mnras/stx421>.
- [42] N. K. Singh, I. Rogachevskii, and A. Brandenburg, *The Astrophysical Journal Letters* **850**, L8 (2017), URL <https://dx.doi.org/10.3847/2041-8213/aa96a1>.
- [43] Z. Yoshida and P. J. Morrison, *Phys. Rev. Lett.* **119**, 244501 (2017), URL <https://link.aps.org/doi/10.1103/PhysRevLett.119.244501>.
- [44] S. Biswas and R. Ganesh, arXiv preprint arXiv:2211.12362 (2022), URL <https://doi.org/10.48550/arXiv.2211.12362>.
- [45] I. Kolokolov, V. Lebedev, and G. Sizov, *Journal of Experimental and Theoretical Physics* **113**, 339 (2011).
- [46] R. Mukherjee, HBNI Phd Thesis (June,2019).
- [47] S. Biswas, R. Ganesh, and et al., *GPU Technology Conference 2022*, <https://www.nvidia.com/en-us/on-demand/session/gtcspring22-s41199/> (2022).
- [48] G. S. Patterson and S. A. Orszag, *The Physics of Fluids* **14**, 2538 (1971), <https://aip.scitation.org/doi/pdf/10.1063/1.1693365>, URL <https://aip.scitation.org/doi/abs/10.1063/1.1693365>.
- [49] A. Gholami, J. Hill, D. Malhotra, and G. Biros, <http://arxiv.org/abs/1506.07933> (2016).
- [50] Paulo-herrera, *PyEVTK*, <https://github.com/paulo-herrera/PyEVTK> (2021).
- [51] LLNL, *VisIt*, <https://wci.llnl.gov/simulation/computer-codes/visit> (2020).
- [52] Kitware, *Paraview*, <https://www.paraview.org/> (2022).
- [53] D. Galloway and U. Frisch, *Geophysical & Astrophysical Fluid Dynamics* **36**, 53 (1986), <https://doi.org/10.1080/03091928608208797>, URL <https://doi.org/10.1080/03091928608208797>.
- [54] S. B. F. Dorch, *Physica Scripta* **61**, 717 (2000), URL <https://doi.org/10.1238/physica.regular.061a00717>.
- [55] Archontis, V., Dorch, S. B. F., and Nordlund, Å., *A&A* **397**, 393 (2003), URL <https://doi.org/10.1051/0004-6361:20021568>.
- [56] I. Bouya and E. Dormy, *Physics of Fluids* **25**, 037103 (2013), <https://doi.org/10.1063/1.4795546>, URL <https://doi.org/10.1063/1.4795546>.
- [57] P. G. Drazin, *Journal of Fluid Mechanics* **10**, 571–583 (1961).
- [58] A. Thess, J. Sommeria, and B. Jüttner, *Physics of Fluids* **6**, 2417 (1994), <https://doi.org/10.1063/1.868189>, URL <https://doi.org/10.1063/1.868189>.
- [59] S. Biswas and R. Ganesh, *Physics of Fluids* **34**, 065101 (2022), <https://doi.org/10.1063/5.0092212>, URL <https://doi.org/10.1063/5.0092212>.
- [60] A. Brandenburg, A. Bigazzi, and K. Subramanian, *Monthly Notices of the Royal Astronomical Society* **325**, 685 (2001).
- [61] N. Leprovost and E.-j. Kim, *The Astrophysical Journal* **696**, L125 (2009).
- [62] A. Courvoisier and E.-j. Kim, *Phys. Rev. E* **80**, 046308 (2009), URL <https://link.aps.org/doi/10.1103/PhysRevE.80.046308>.
- [63] Y. B. Zeldovich, *Sov. Phys. JETP* **4**, 460 (1957).
- [64] L. K. Currie and S. M. Tobias, *Geophysical &*

Astrophysical Fluid Dynamics **113**, 131 (2019), <https://doi.org/10.1080/03091929.2018.1517210>, URL <https://doi.org/10.1080/03091929.2018.1517210>.
 [65] S. A. Balbus and J. F. Hawley, Rev. Mod. Phys. **70**, 1 (1998), URL [https://link.aps.org/doi/10.1103/](https://link.aps.org/doi/10.1103/RevModPhys.70.1)

<https://doi.org/10.1080/03091929.2018.1517210>.
 [66] J.-F. Donati, F. Paletou, J. Bouvier, and J. Ferreira, nature **438**, 466 (2005), URL <https://doi.org/10.1038/nature04253>.

Appendix A: Benchmarking of GMHD3D solver

We have looked into the kinematic dynamo problem for a class of ABC flow at different magnetic Reynolds numbers. The velocity profile for ABC flow is given by,

$$\begin{aligned} u_x &= [A \sin(y) - C \cos(z)] \\ u_y &= [B \sin(z) - A \cos(x)] \\ u_z &= [C \sin(x) - B \cos(y)] \end{aligned} \tag{A1}$$

where the choice of A, B, C values are 1. When we use this initial condition, we obtain the identical exponential growth in magnetic energy like Galloway and Frisch^[53]. The three-dimensional visualization of the magnetic energy iso-surface reveals “cigar-like” structures, which represent the fastest-growing growth mode [See Fig. 9].

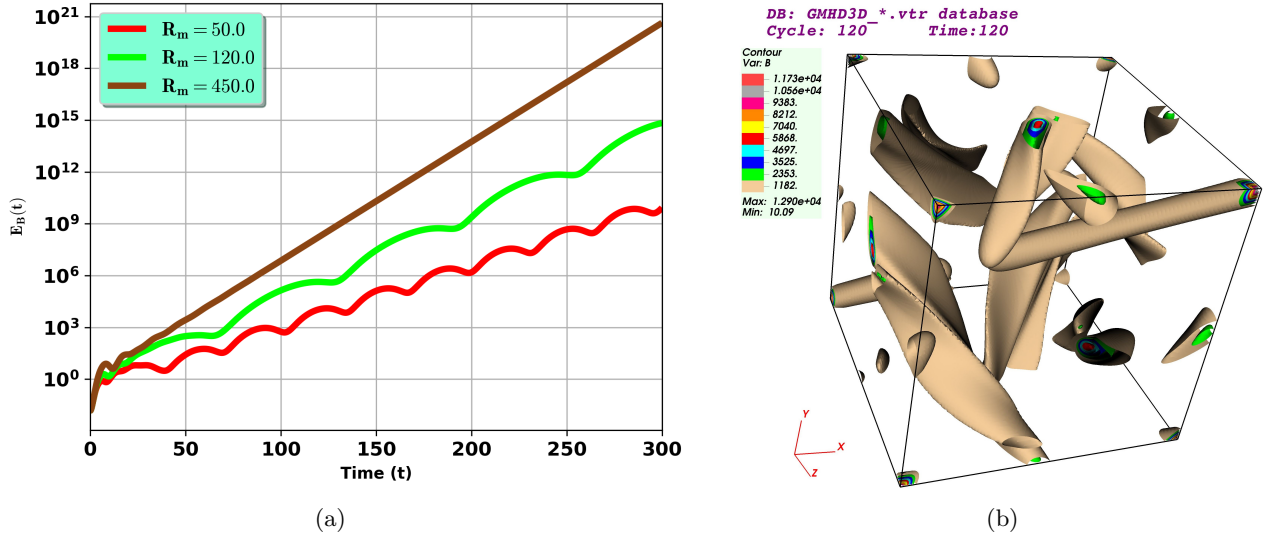
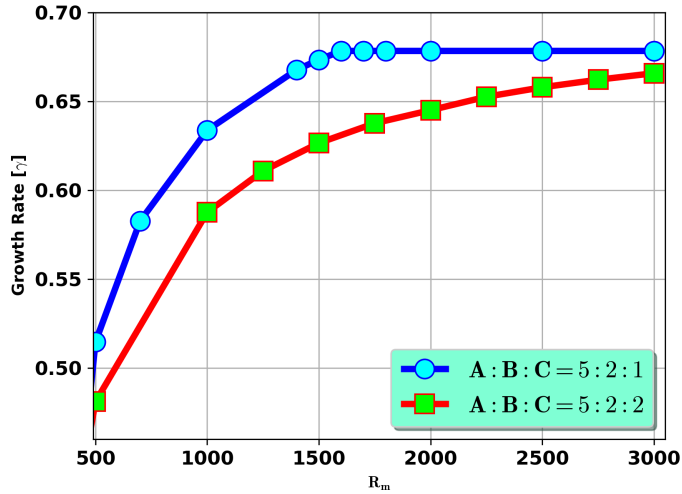
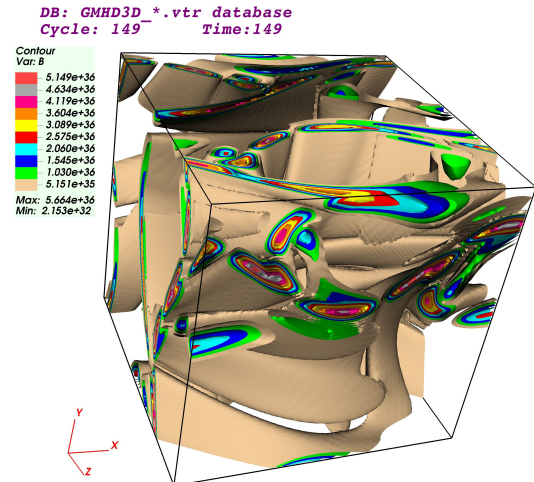


FIG. 9: (a) Time evolution of magnetic energy (E_B) for different values of magnetic Reynolds numbers. (b) Magnetic energy iso-surface visualization leads to concentrated “cigar like” structures. The identical observation was reported by Galloway and Frisch^[53].

We have also used ABC flow to study the properties of kinematic dynamos, but with a slightly distinct topology. We have investigated the case where A, B, C is 5, 2, 2 and found that in the latter instance, the magnetic field is amplified exponentially, with the growth rate increasing with R_m . However, in the 5, 2, 1 scenario, it is discovered that the growth rate of magnetic energy reaches a maximum at a value of 0.67. Archontis et al^[55] also found something very close to this. The “cigar-like” structures that form in the classical $A = B = C = 1$ case are substituted with “ribbon-like” structures [See Fig. 10].



(a)



(b)

FIG. 10: (a) Magnetic energy growth rate (γ) versus the magnetic Reynolds number (R_m) for the $5 : 2 : 1$ & $5 : 2 : 2$ flow. (b) The magnetic energy iso-surface looks like ribbons when $A : B : C = 5 : 2 : 2$. This observation is identical to Archontis et al⁵⁵.